Journal of
Synchrotron Radiation

ISSN 0909-0495

Received 11 April 2012
Accepted 24 May 2012

Advantages of a synchrotron bending magnet as the sample illuminator for a wide-field X-ray microscope

M. Feser,[a]* M. R. Howells,[b] J. Kirz,[b] J. Rudati[a] and W. Yun[a]

[a]Xradia, 4385 Hopyard Road, Suite 100, Pleasanton, CA 94588, USA, and [b]Advanced Light Source, Lawrence Berkeley National Laboratory, 1 Cyclotron Road, Berkeley, CA 94720, USA.
E-mail: mfeser@xradia.com

In this paper the choice between bending magnets and insertion devices as sample illuminators for a hard X-ray full-field microscope is investigated. An optimized bending-magnet beamline design is presented. Its imaging speed is very competitive with the performance of similar microscopes installed currently at insertion-device beamlines. The fact that imaging X-ray microscopes can accept a large phase space makes them very well suited to the output characteristics of bending magnets which are often a plentiful and paid-for resource. There exist opportunities at all synchrotron light sources to take advantage of this finding to build bending-magnet beamlines that are dedicated to transmission X-ray microscope facilities. It is expected that demand for such facilities will increase as three-dimensional tomography becomes routine and advanced techniques such as mosaic tomography and XANES tomography (taking three-dimensional tomograms at different energies to highlight elemental and chemical differences) become more widespread.

Keywords: TXM microscope; bending-magnet beamline; synchrotron beamline design; X-ray microscope.

1. Background

Synchrotron-based zone-plate X-ray microscopes are of two main types, the transmission X-ray microscope (TXM) and the scanning transmission X-ray microscope (STXM). Both types have been in use on synchrotrons for more than three decades and have been reviewed for example by Kirz *et al.* (1995), Howells *et al.* (2007), Kaulich *et al.* (2011) and Falcone *et al.* (2011). The recent history of the field can be followed *via* a triennial series of international conferences running from 1983 to the present. For the three most recent, see Aoki *et al.* (2006), David *et al.* (2009) and McNulty *et al.* (2011). In the 2007 review by Howells *et al.* (2007), 26 such microscopes worldwide are tabulated. There are 12 TXMs, seven on insertion devices and five on bend magnets, and 14 STXMs, all but one of which are on undulators. To our knowledge at the time of writing, the number of TXMs has grown to 18 with 11 on insertion devices and seven on bending magnets. It is understandable that almost all STXMs use an undulator because, for those instruments, the zone plate requires coherent illumination in order to achieve its diffraction-limited resolution and undulators have the highest coherent power. On the other hand, for TXMs, there is no such coherence requirement and the measure of source strength is the rate of delivery of flux into a phase-space volume equal to the phase-space acceptance of the microscope (we will explain this more quantitatively below). Of course an insertion device will almost always have a flux advantage when measured in this way. Nevertheless, in many cases it would still be preferable to use a bending-magnet beamline for practical and cost reasons, provided it could deliver adequate flux for the intended application. A principal reason why the balance of factors is tilted toward the bend magnet is that the task of modifying both the size and shape of the phase-space volume of the insertion-device beam to optimally match that of the microscope can be challenging from both a technical and program planning point of view. In this paper we investigate further this choice between bending magnets and insertion devices as sample illuminators for a TXM.

In most cases insertion devices and their beamlines are individually designed to utilize storage-ring straight sections and are regarded as scarce and expensive resources. On the other hand, bending-magnet sources are much less expensive and many more of them are available. This makes the idea of a bending-magnet beamline, *dedicated* to a TXM, easier to justify. It is clear from the above that the potential flux advantages of insertion-device beamlines will not be realised unless they are optimally phase-space matched to the TXM. It is therefore reasonable to ask if existing insertion-device beamlines that feed a TXM are really optimally matched. In

fact we believe that, for various reasons, they usually are not. This could be because the insertion device and beamline are inherited from an earlier program or are shared with another experiment, or the technical difficulties of achieving optimal matching have led to a compromise optical design. In such cases the flux advantage is reduced or eliminated, and the realistic option of a bending-magnet beamline, that *is* purpose-designed and optimally matched to a TXM, become much more competitive. We investigate this more quantitatively in the following.

2. Introduction

We have recently carried out a study of three-dimensional X-ray imaging for non-destructive inspection of microcircuits. The study (Xradia, 2010), which we will refer to as XR2010, demonstrates in detail, both experimentally and by computer modelling, that a TXM using 9 keV X-rays delivered by an optimized bending-magnet beamline on any of the five synchrotrons run by the USA Department of Energy can broadly match the imaging speeds of existing TXMs installed on undulator or wiggler beamlines. The essential goal was to establish the feasibility of a dedicated beamline facility to use X-ray computed tomography to non-destructively image microcircuits in three dimensions for failure analysis, and design verification. The detailed methods and conclusions of the study are described elsewhere (Xradia, 2010). Here we emphasize the insights that emerged from the study, that bear on more general beamline design issues.

In the following we outline the basic assumptions and design principles of a TXM beamline and we describe our proposed generic beamline design, known as the 'coma-corrected toroid' (CCT) system, which incorporates Codling slits and is suited for the crystal-optics energy range. We then use the results of some of our experimental work, carried out at the Stanford Synchrotron Radiation Laboratory (SSRL), to determine a benchmark for adequate X-ray *illumination* of a microcircuit for eventual production of a 'good' tomogram and three-dimensional image as an application example. (The benchmark is a general requirement that applies to any illumination set-up, but was first determined using images made using the Xradia NanoXCT-S100 microscope at the SSRL 54-pole wiggler, beamline 6.2.) For other applications the absolute photon numbers required might be different, but the conclusions on the exposure times, with one source, *relative* to that with another, will still be valid.

We then use the calculated time needed to deliver the benchmark illumination as a figure of merit for assessing the microcircuit-imaging capability of the combination of our CCT beamline scheme with bending-magnet sources. Of course, the operating parameters of synchrotrons and their bending magnets vary considerably, so to gain insight into how imaging capability varies over different synchrotrons our study made comparative assessments for five American synchrotron facilities. To do this fairly, we chose the parameters of our CCT beamline design to optimally match the published source characteristics and floor layout constraints of each of the following sources: the National Synchrotron Light Sources I and II (NSLS-I and NSLS-II), the Advanced Photon Source (APS), the Advanced Light Source (ALS) and SSRL. We then calculated the exposure times needed for the benchmark illumination in each case. We report these calculations in detail below and discuss the results in light of our experimental results with the SSRL wiggler.

3. Basic design principles for an X-ray microscope beamline

3.1. Illumination of the sample

The output beam of a synchrotron radiation X-ray source is characterized by the full width (h) and the full angle (h') of the X-ray beam in the horizontal plane and similarly by v and v' in the vertical plane. [For Gaussian distributions we use the full width at half-maximum (FWHM).] Other important quantities are the horizontal and vertical *emittances*, $\varepsilon_{\rm h}$ and $\varepsilon_{\rm v}$ of the X-ray beam, defined by

$$\varepsilon_{\rm h} = hh' \qquad \text{and} \qquad \varepsilon_{\rm v} = vv'. \tag{1}$$

The emittance is an important descriptor of the beam in that it is invariant under linear optical processes such as magnification. For TXM operation the beamline must be designed to match the emittances of the X-ray beam to the *acceptances* of the microscope in both horizontal and vertical planes. The horizontal acceptance of the microscope, $\varepsilon_{\rm h}^{\rm M}$, is defined, analogously to $\varepsilon_{\rm h}$, as the product of the horizontal sample width to be illuminated and the horizontal angle (at the sample plane) needed to fill the microscope lens with light (and similarly for the vertical acceptance).

3.2. Choice of the width and angle of the X-ray beam required by the microscope

The penetration required for imaging microcircuits with a silicon substrate thickness of approximately 100 µm implies that hard X-rays need to be employed and the type of contrast (mostly copper against a background of silicon) suggests that amplitude (absorption) contrast will be predominant. The case we studied in XR2010 used 9 keV illumination for best compromise of transmission and contrast and a field of view (FOV) of 40 µm × 40 µm was selected, limited by the resolving power of the X-ray optics and desired sample-plane pixel size of 20 nm with a 2k sensor. (We will see that the desired practical resolution is 50 nm.)

For optimal microscope resolution the convergence angle of the sample illumination is chosen to match the full angle of 5 mrad [equal to twice the numerical aperture (NA)] accepted by the zone-plate objective lens (Meyer-Ilse *et al.*, 1995). The microscope optical system is schematically illustrated in Fig. 1, while the calculation of the actual X-ray beam widths and angles compared with the *desired* widths and angles to match the microscope are explained in Fig. 2.

The optimal matching, that we have alluded to, requires matching not only the *sizes* of the phase-space volumes $\varepsilon_{\rm h}$ and $\varepsilon_{\rm h}^{\rm M}$ or $\varepsilon_{\rm v}$ and $\varepsilon_{\rm v}^{\rm M}$ by 'stretching' $\varepsilon_{\rm h}$ or $\varepsilon_{\rm v}$ (see next section) but

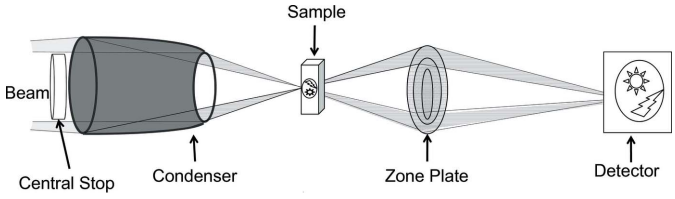

Figure 1
Schematic diagram of the illumination of the sample area.

also their *shapes* at the sample plane, *i.e.* the beam spot size must match the FOV and its angle must match 2NA (Fig. 2).

3.3. Unavoidable mismatch of the beamline emittance and microscope acceptance

With most synchrotron light sources the emittance is too small in the vertical plane (and sometimes in both planes) to match the microscope acceptance, hence either only part of the sample area is illuminated or the beam angle underfills the objective lens, or both. Since the beam emittance is not changed by a magnification, the mismatch cannot be overcome by optical design. However, several schemes have been implemented that do overcome the problem. Generally this involves *sequentially* filling the acceptance area either by scanning the position or angle of an optical element in the beamline or in the microscope. In the examples shown below, such a process is used to effectively 'stretch' the emittance ε_v to equal ε_v^M. With stretching, the exposure takes approximately the same time it would have taken if the same amount of flux had been spread evenly over the acceptance width or angle, *i.e.* if the emittance and acceptance had happened to match naturally.

While insertion-device sources have much higher brightness [more photons per unit time per emittance volume ($\varepsilon_h\varepsilon_v$) per unit fractional bandwidth], bending-magnet sources provide larger emittance, especially in the horizontal plane and to a smaller extent in the vertical plane (compared with undulators), hence the mismatch between emittance and acceptance is reduced. This is one reason why bending magnets can be made competitive with brighter insertion devices for full-field X-ray microscopy.

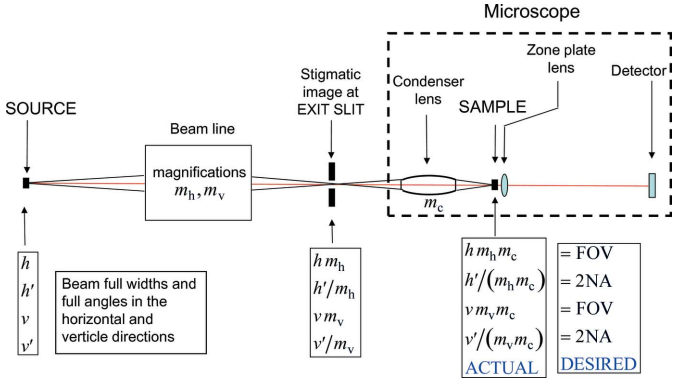

Figure 2
Actual beam widths and angles at various positions on the beamline and their dependence on the magnifications m_h and m_v of the beamline and m_c of the condenser. The actual values at the sample plane are compared with their *desired* values.

3.4. A bending-magnet beamline for a TXM: design goals

The goal of the optical designer is to make sure that the X-ray beam delivered to the sample plane fills the desired width and angle in both planes using scanning of optical components if necessary. We treat specific issues arising in the use of the CCT beamline with a capillary condenser in §6.2. The other principal requirement is not to waste X-rays, so we must design the optics so that the secondary source, that is the image of the real source delivered by the beamline to the exit slit (that the condenser lens will subsequently demagnify onto the sample), will not be significantly blurred by the aberrations of the optical system or manufacturing errors in the reflecting optical components. The main point of the CCT design is to ensure this while keeping the design as simple as possible for cost reasons. Attention must also be paid to the efficiencies of all of the optical components.

4. The 'coma-corrected-toroid' beamline design

We propose a simple beamline design which consists of a parabolic mirror that collimates the beam in the vertical direction, a double-crystal monochromator to provide a working energy of 9.0 keV, and a toroidal focusing mirror that focuses the beam in both directions onto an exit slit as illustrated in Fig. 3. The beam emerging from the exit slit illuminates the microscope condenser. As we will see, negligible aberration losses at the exit slit can be achieved by an optimum choice of the imaging conjugates of the toroidal mirror. The phase space of the bending-magnet X-ray sources considered in XR2010 allow exact matching to the microscope acceptance in the horizontal so the width and angle of the beam arriving at the sample are correct in those cases. However, in the vertical the beam width and angle are both too small and must be increased by scanning.

4.1. Mirrors

The purpose of the collimating mirror is to provide parallel illumination in the vertical plane to match the need of the vertically deflecting double-crystal monochromator. It is a

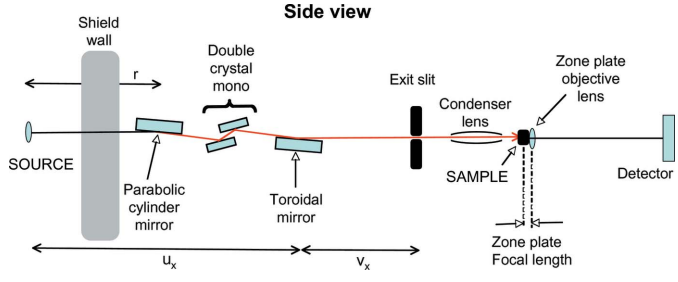

Figure 3
CCT beamline schematic. Good imaging at the exit slit is obtained when the horizontal beamline magnification $m_h = v_x/u_x = 0.5$. In the vertical $m_v = v_x/r$ which is constrained to be reasonably near to unity as explained in §4.5.

Table 1
Zone-plate parameters.

Item	Unit	Value
X-ray energy	keV	9.0
Outer zone width	nm	30
Radius	μm	100
Number of zones		1667
Focal length (at X-ray energy)	mm	43.6
Numerical aperture (at X-ray energy)	mrad	2.30
Rayleigh resolution	nm	36.6†
Efficiency (measured)	%	10

† Intended practical resolution requirement = 50 nm.

Table 2
Parameters of the asymmetric-cut monochromator.

Item	Unit	Value
Crystal		Si 111
X-ray energy	keV	9.0
Bragg angle	°	12.69
Cut surface angle to 111 surface	°	10.31
First crystal incident angle†	°	2.38
First crystal outgoing angle†	°	23
Energy resolution ($\Delta E/E$)		1/2400
Increase factor in flux relative to Si 111		2.9
Increase factor in flux relative to Si 220		6.6
Crystal length	mm	100

† These angles are reversed on the second crystal.

parabolic cylinder, most easily obtained by gently bending an optical flat to the desired shape. The focusing mirror collects the monochromatic beam (optically unaffected by the double-crystal monochromator) and must deliver a stigmatic focus at the exit slit. The mirror must therefore be toroidal, a shape that is most easily obtained by gently bending a cylindrical mirror. It is noteworthy that the beam received by the toroidal mirror is parallel in the vertical direction and is diverging from the synchrotron source in the horizontal. The toroidal mirror has therefore a *cylindrical* incoming wavefront and (because of the requirement for a stigmatic focus at the exit slit) a spherical outgoing wavefront. This is unusual and cannot be analyzed by the standard tabulated aberration terms (see, for example, Noda *et al.*, 1974; Padmore *et al.*, 1998; Howells, 2001), which are based on nominal point-to-point imaging. Rather, an analysis based on *line*-to-point imaging must be used. This has been worked out and shows that the lowest-order coma-type aberration is exactly corrected when the toroid magnifications (M) are at the 'magic' values $\{M_V = 0, M_H = 1/2$ leading to much improved image quality. This is analogous to a similar, well known, aberration correction that occurs for the magic values $M_V = M_H = 1$ in the point-to-point imaging case. More detail and ray traces of this scheme are shown by Padmore (2000) and MacDowell *et al.* (2004). The design is becoming quite popular, and has been successfully implemented on several beamlines such as the three Advanced Light Source (ALS) super-bend crystallography beamlines 8.2.1, 8.2.2 and 8.3.1 (MacDowell *et al.*, 2004).

4.2. The monochromator and bandwidth selection

The zone plate used as microscope objective is a diffractive and hence chromatic optical element. To avoid resolution degradation, the illumination must be monochromatic. Roughly speaking, the fractional bandwidth should be less than the reciprocal of the number of zones in the zone plate (Thieme, 1988). For our experiments at SSRL, a zone plate with 200 μm diameter, 30 nm finest zone and about 1700 zones (Table 1) has been used successfully. A monochromator of resolving power ∼2000 is therefore suitable to achieve full resolution in the images.

The double-crystal monochromator could use standard Si(111) crystals. However, the bandwidth in that case would be about a factor of four smaller than the required $\Delta E/E$ = 1/2000, implying a factor of four loss of flux. Hence we propose to use asymmetrically cut crystals which have a wider bandwidth and thereby regain most of the available flux (Hastings, 1977; Hastings *et al.*, 1978; Nave *et al.*, 1995). The calculated gain factors for the area under the rocking curve (giving the flux) and its FWHM (giving the fractional bandwidth) are shown in Fig. 4 as a function of the cut angle. The asymmetrically cut monochromator optimized for 9 keV imaging will have the following parameters: crystal surface cut at 10.31° with respect to the 111 surface, incident grazing angle on the first crystal of 2.38°, and outgoing angle of 23.00° (Table 2). On the second crystal these angles are reversed. This corresponds to an increase in bandwidth by a factor of 3.3 and a cut angle which experience shows is as close to the Bragg angle as one can go without suffering losses due to the surface imperfections of practical crystals. The monochromator produces a vertical offset of about 2 cm and has no focus–defocus properties. Thus the beam is horizontal and also collimated in the vertical plane both before and after the monochromator, the position of which can, therefore, be anywhere between the two mirrors.

4.3. Codling slit

The unusual component of our beamline design is the exit slit. As noted above, the beam emittance and microscope acceptance could be matched in the horizontal and the exit slit filled with a beam of the correct size and angle. In the vertical

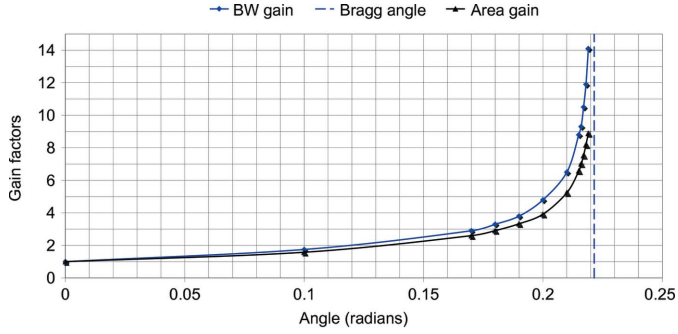

Figure 4
Gain factors for width and area of the rocking curve owing to an asymmetric cut as a function of the cut angle to the Bragg plane. Calculation was by the Darwin–Prins method for a silicon 111 crystal in *s*-polarization delivering 9 keV X-rays.

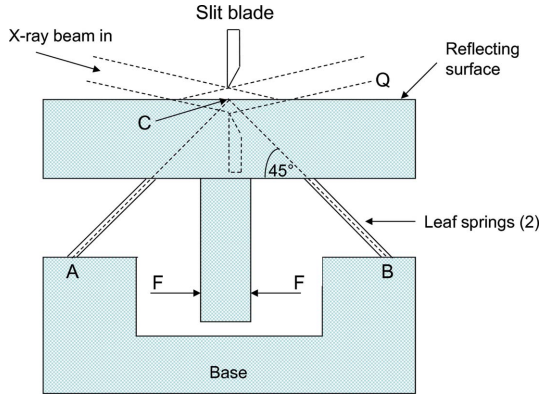

Figure 5
Diagram suggesting how a rotatable Codling slit might be realised. A reciprocating force is applied at points F which causes the springs to bend so that the mirror rotates back and forth about point C at the center of the reflecting surface. The arrangement behaves as though the image of the slit blade is a real blade as can be seen from ray Q which appears to come from the point of the blade image.

plane, however, the angular range of the beam was always too small by more than an order of magnitude to fill the circular entrance aperture of the condenser. In order to spread the angles to the required range, we adopt a dynamic implementation of the slit design introduced by K. Codling (Codling & Mitchell, 1970) that is used in several soft X-ray monochromator systems. In Codling's slit design, one of the vertical edges of the slit is replaced by a small plane mirror as illustrated in Fig. 5. This mirror is slightly inclined with respect to the optical axis so as to intercept all the beam that passes through the slit. Furthermore, the mirror is made to rotate slightly (about ± 1 mrad in our examples) around a pivot axis at the intersection of the mirror and slit planes. The rotation sweeps the beam back and forth to fill the ingoing angle of the condenser and therefore also its outgoing angle which is delivered to the sample (see Fig. 5). The scanning frequency of the mirror should be chosen to be as high as possible (compared with the exposure time of the microscope which is in the 1 s range) to obtain a sufficient amount of time averaging of the illumination. To our knowledge, such a dynamically scanned Codling slit has not yet been demonstrated in practice. We note also that the fact that the X-ray beam is monochromatic at the Codling slit reduces concerns about radiation-induced carbon contamination, which has been a concern in the past when implementing a stationary Codling slit at the *entrance* of a monochromator. In the horizontal direction a pair of static blades is employed to define the beam.

4.4. Microscope condenser

The microscope condenser is a single-reflection capillary mirror, with the inside surface figured to an ellipsoid of revolution (Zeng *et al.*, 2008). It relays the beam emerging from the slit onto the sample on the microscope stage. Owing to the Codling slit, the capillary sees a beam that appears to emerge from a normal slit pair with four blades. Owing to the rapid wobbling of the Codling mirror, the vertical extent of the illumination on the condenser is increased to fill the aperture of the condenser and match the horizontal beam size. Additionally, the condenser position will also be scanned in a pure vertical translation to fill the entire FOV in the sample plane in the vertical direction (in the case considered the amplitude is $\sim$<40 µm to fill the 40 µm FOV). To block rays arriving at the condenser that would pass without bouncing on the ellipsoidal surface, a central stop is used, which intercepts approximately 50% of the beam as illustrated in Fig. 1 and creates a hollow-cone illumination, which is required in a zone-plate microscope owing to the presence of other diffraction orders.

4.5. Detailed considerations for phase-space matching a CCT beamline to a TXM with a capillary condenser

In all the examples treated here the available X-ray beam emittance in the horizontal direction from a bending magnet is always larger than the required microscope acceptance. One can therefore match these in the horizontal plane by using the collection angle from the bending-magnet source as an adjustable parameter h'. This is in practice implemented by the choice of mirror widths and the use of additional slits in the beamline. Using notation from Fig. 2, the overall magnification (source to sample) is $m_{\rm h}m_{\rm c} = {\rm FOV}/h$. Moreover, in the case of the CCT design we must have $m_{\rm h} = 0.5$ from which the condenser horizontal magnification is also fixed. Given the circular symmetry of the condenser, its magnification in both planes is therefore fixed. Actual values of the quantities known in advance are given in Table 3. The need for scanning both the vertical position and angle arises because the condenser vertical magnification has been fixed by the horizontal matching process and the vertical beamline magnification ($m_{\rm v} = v_x/r$) is constrained to values reasonably near to unity owing to the layout of components on the synchrotron floor. The simplest beamline layout beginning at the source and ending at the exit slit has the two mirrors placed at the one-third and two-thirds points (see Fig. 3). This leads to $m_{\rm h} = 0.5$ (required) and $m_{\rm v} = 1$ and the total length of the beamline is three times the source-to-first-mirror distance (r). To make $m_{\rm v}$ greater than unity one would need to either reduce r, which would be constrained by shield-wall limits *etc.*, or increase v_x by some factor, which would lengthen the whole beamline by the same factor.

5. Criteria for X-ray illumination conditions for satisfactory three-dimensional imaging of copper interconnects in microcircuits

The following parameters have been identified as required for obtaining high-fidelity images of the copper interconnect structure of 90 nm node microcircuits used as an example in this paper: (i) resolution $\leq$ 50 nm; (ii) X-ray energy = 9 keV; (iii) number of X-rays per unit area per two-dimensional exposure (projection image) $\geq$ 120 nm^{-2}; (iv) two-dimensional image exposure time of $\sim$1 s (reference image without sample); (v) number of exposures (projections) per three-dimensional dataset $\geq$ 120.

Table 3
Parameters for TXM beamlines.

Parameter	Unit	NSLS I	NSLS II-WIG	APS	ALS-SB	SSRL
Storage ring						
Energy	GeV	2.8	3.0	7.0	1.9	3.0
Current	mA	300	500	100	500	500
Brightness	photons s^{-1} $mrad^{-2}$ mm^{-2} (0.1% bandwidth)$^{-1}$	4.3×10^{14}	2.9×10^{15}	5.4×10^{15}	2.6×10^{15}	1.3×10^{15}
Source size (h × v)	μm	638 × 134	568 × 39	232 × 60	266 × 35	451 × 120
Source angle (h × v)	mrad	0.31 × 0.24	0.35 × 0.22	0.86 × 0.17	0.75 × 0.51	0.44 × 0.24
Beamline						
Vertical demagnification (r/v_x)		1.0	1.56	1.44	1.0	1.0
Horizontal demagnification† (u_x/v_x)		2.0	2.0	2.0	2.0	2.0
Slit opening (h × v)	μm	319 × 134	239 × 25	116 × 42	133 × 35	225 × 120
Beam height at optics	mm	2.2	6.2	3.9	3.3	3.0
Beam width at toroid	mm	5.6	23.5	40	9.8	11
Microscope						
Condenser demagnification‡		8.0	6.0	2.9	3.3	5.6
Illumination angle‡	mrad	5.0	5.0	5.0	5.0	5.0
FOV§ (h × v)	μm	40 × 40	40 × 40	40 × 40	40 × 40	40 × 40
Spot scan distance vertically	μm	25	35	20	30	20
Angle scan vertically	mrad	1.3	5.4	3.3	5.7	1.7
Time to benchmark illumination	s	1.6	0.94	0.42	0.50	0.59
Floor layout						
Collimator distance¶	m	9.0	28	23	6.5	12.5
Monochromator distance	m	11.0	32	27.5	10	15
Toroidal mirror distance	m	18	36	32	13	25
Exit slit distance	m	27	54	48	19.5	37.5

† Source to exit slit. ‡ Same in horizontal and vertical. § FOV = field of view. ¶ All floor distances are measured from the source.

These conditions are based on datasets taken during the last three years using an Xradia nanoXCT-S100 X-ray microscope installed at beamline 6-2 at SSRL fed by a 54-pole wiggler (Andrews *et al.*, 2008). The above illumination conditions were met in those experiments. However, it is important to note that these are general criteria that must be met by *any* illumination system that is intended to be used for this application with the same throughput. In the following we will investigate what is required to meet these same criteria using a bending-magnet source.

6. Comparison of sources

6.1. Definition of the sources to be compared

The NSLS-I source is hosting an Xradia UltraXRM-S200 microscope on the existing X8C bending-magnet beamline (Alkire *et al.*, 1995) which started to operate in 2011, albeit not with an optimized beamline configuration. NSLS-I is a relatively old source, and this is reflected in relatively large source sizes. Around 2015 NSLS-I will be replaced by the state-of-the-art new light source NSLS-II. The bend magnets of this storage ring will be too weak for practical use at 9 keV; however, there will be a number of three-pole wigglers available, and the parameters below assume that the source is one of those. The APS is the highest-energy light source operating in the USA. It offers high brightness, and over the next decade it is expected to undergo an upgrade that will further improve its performance. The design listed here is based on the current status. The ALS is a low-energy storage ring, designed mostly for soft X-ray applications. It does offer several 'superbend' sources, however, where superconducting magnets are used to provide hard X-ray beams. Our calculations assume one of these superbend sources. SSRL has already been upgraded and is approaching the point where it will be running at 500 mA current in top-off mode. The calculations assume this mode of operation.

6.2. Defining the parameters of the CCT beamline: matching the phase space

Our approach is to utilize the published source characteristics[1] and floor layout of each storage ring to choose those parameters of the CCT beamline design that are available to be chosen. In all of these five cases it proved possible to use the horizontal collection angle as a free parameter to match the beam emittance to the microscope acceptance in the horizontal plane. Since the horizontal magnification of the beamline must be 0.5 (§4.1), this allows the horizontal (and necessarily also the vertical) magnification of the condenser lens to be determined. Moreover, the beamline vertical magnification (v_x/r in Fig. 3) is limited by floor-layout considerations to values reasonably near to unity (*e.g.* about 0.6 to 1.3). This limitation results from our use of the CCT

[1] Argonne, http://www.aps.anl.gov/Beamlines/Directory/; Brookhaven, http://www.bnl.gov/nsls2/project/source_properties.asp; Stanford, http://ssrl.slac.stanford.edu/userresources/beamlines/beamlines.html; ALS, http://www-als.lbl.gov/index.php/beamlines/photon-source-parameters/368-storage-ring-parameters.html).

beamline design and has the consequence that the vertical phase-space has to be stretched, both in angle, using the Codling slit, and in spot size, by scanning the condenser position. The spot scan is necessary because to obtain a spot of height FOV at our chosen sources would require m_v values ranging from 1.9 to 6.2 which are outside the allowed range. This type of double scan is unusual and is not required in other TXM beamlines, particularly in the soft X-ray region, where the vertical magnification is less constrained.

Including scanning the final result at the sample plane must be that the area illuminated is 40 μm × 40 μm, and the full angular extent of the beam is 5 mrad × 5 mrad to match the zone-plate numerical aperture of ∼2.5 mrad. This information is summarized in Table 3. The table essentially defines five hypothetical beamline designs, all of which are intended for 9.0 keV operations.

6.3. Results and discussion of the comparison

The result of the comparison as measured by the exposure time to achieve benchmark illumination of the sample is simple. The oldest source NSLS-I requires the longest time but is still less than a factor of four different from the shortest time, achieved by APS. Thus all five times are in the range 0.42 to 1.6 s. So, bearing in mind 'non-exposure' overheads, these times can be considered to be quite close. We also note that they are all close to the benchmark exposure time of 1 s achieved (experimentally) by the 54-pole wiggler at Stanford.

Evidently our calculated times for benchmark illumination for purpose-designed bending-magnet beamlines using the CCT optical scheme do approximately match the (measured) performance of the 54-pole wiggler. We might ask why the wiggler did not perform better. It is, after all, roughly equivalent to 54 bending magnets. The reason, as we discussed in the *Introduction*, is because the wiggler and beamline were not purpose-built for the TXM. Thus, although the beamline is dedicated to the TXM, it is not phase-space-matched. In fact, the developers of the SSRL TXM facility knew that the *pre-existing* wiggler and *pre-existing* beamline that they were planning to use would allow the TXM to accept only 2–4% of the horizontal phase space of the wiggler (Pianetta, 2009). But they also knew that with 54 poles they would still have a viable microscope facility, as has now been amply demonstrated. With this understanding one can see why a bending-magnet beamline could be competitive. One can also see the importance of using a beamline that is purpose-designed for a TXM. We may therefore summarize our technical conclusions as follows.

6.4. Technical key points

Insertion-device beamlines are rarely optimally phase-space matched to TXMs.

The consequence of not being matched is normally a large loss of the potentially available flux.

Almost any bending magnet on a present-day storage ring (with a suitable X-ray energy spectrum) can be phase-space matched to a TXM and deliver performance that is competitive with the same TXM on an unmatched insertion-device beamline.

7. General conclusions

We believe that we have shown convincingly that, through optimization of the selection and arrangement of beamline components, bending-magnet synchrotron sources can deliver a throughput of X-ray microscope images that is very competitive with the performance of similar microscopes installed currently at insertion-device beamlines. The fact that imaging X-ray microscopes can accept a large phase space makes them very well suited to the output characteristics of bending magnets which are often a plentiful and paid-for resource. There exist opportunities at all synchrotron light sources to take advantage of this finding to build bending-magnet beamlines that are dedicated to transmission X-ray microscope facilities. It is expected that demand for such facilities will increase as three-dimensional tomography becomes routine and advanced techniques such as mosaic tomography and XANES tomography (taking three-dimensional tomograms at different energies to highlight elemental and chemical differences) become more widespread.

It is also noteworthy that most of our findings in this work have been expressed as statements about bending-magnet sources *relative* to insertion devices. The findings are consequently applicable to all sample types, not only to microcircuits, and to all X-ray energies delivered by the CCT beamline, not only to 9 keV.

We are pleased to acknowledge support from a DARPA Seedling Grant, subcontract GTS-S-10-1-008. It is also a pleasure to acknowledge the capable help of the SSRL beamline 6.2 team and valuable discussions with Dr P. Pianetta. The views expressed are those of the authors and do not reflect the official policy or position of the Department of Defence or the US Government. This is in accordance with DoDI 5230.29, 8 January 2009. Approved for Public Release, Distribution Unlimited.

References

Alkire, R. W., Sagurton, M., Michaud, F. D., Trela, W. J., Bartlett, R. J. & Rothe, R. (1995). *Nucl. Instrum. Methods Phys. Res. A*, **352**, 535–541.

Andrews, J. C., Brennan, S., Patty, C., Luening, K., Pianetta, P., Almeida, E., van der Meulen, M. C. H., Feser, M., Gelb, J., Rudati, J., Tkachuk, A. & Yun, W. (2008). *Synchrotron Radiat. News*, **21**, 17–26.

Aoki, S., Kagoshima, Y. & Suzuki, Y. (2006). Editors. *Proceedings of the 8th International Conference on X-ray Microscopy*, Himeji, Japan. Tokyo: Instute of Pure and Applied Physics.

Codling, K. & Mitchell, P. (1970). *J. Phys. E*, **3**, 685–689.

David, C., Nolting, F., Pfeiffer, K., Quitmann, C. & Stamanoni, M. (2009). Editors. *Proceedings of the 9th International Conference on X-ray Microscopy*, Zürich, Switzerland. (*J. Phys. Conf. Ser.* **186**.)

Falcone, R., Jacobsen, C., Kirz, J., Marchesini, S., Shapiro, D. & Spence, J. (2011). *Contemp. Phys.* **52**, 293–318.

Hastings, J. B. (1977). *J. Appl. Phys.* **48**, 1576–1585.

Hastings, J. B., Kincaid, B. M. & Eisenberger, P. (1978). *Nucl. Instrum. Methods*, **152**, 167–171.
Howells, M. R. (2001). In *X-ray Data Booklet* (LBNL/PUB-490, revision 2), edited by A. C. Thompson and D. Vaughan. Lawrence Berkeley National Laboratory, Berkeley, CA, USA.
Howells, M. R., Jacobsen, C. J. & Warwick, T. (2007). In *Science of Microscopy*, edited by P. Hawkes and J. C. H. Spence. New York: Springer.
Kaulich, B., Thibault, P., Gianoncelli, A. & Kiskinova, M. (2011). *J. Phys. Condens. Matter*, **23**, 083002.
Kirz, J., Jacobsen, C. & Howells, M. (1995). *Q. Rev. Biophys.* **28**, 33–130.
MacDowell, A. A., Celestre, R. S., Howells, M., McKinney, W., Krupnick, J., Cambie, D., Domning, E. E., Duarte, R. M., Kelez, N., Plate, D. W., Cork, C. W., Earnest, T. N., Dickert, J., Meigs, G., Ralston, C., Holton, J. M., Alber, T., Berger, J. M., Agard, D. A. & Padmore, H. A. (2004). *J. Synchrotron Rad.* **11**, 447–455.
McNulty, I., Eyberger, C. & Lai, B. (2011). Editors. *10th International Conference on X-ray Microscopy*, Chicago, USA. (*AIP Conf. Proc.* **1365**.)
Meyer-Ilse, W., Medecki, H., Jochum, L., Anderson, E., Attwood, D., Magowan, C., Balhorn, R. & Moronne, M. (1995). *Synchrotron Radiat. News*, **8**, 29–33.
Nave, C., Clark, G., Gonzalez, A., McSweeney, S., Hart, M. & Cummings, S. (1995). *J. Synchrotron Rad.* **2**, 292–295.
Noda, H., Namioka, T. & Seya, M. (1974). *J. Opt. Soc. Am.* **64**, 1031–1036.
Padmore, H. A. (2000). ALS internal report LSBL-548. Advanced Light Source, Berkeley, CA, USA.
Padmore, H., Howells, M. R. & McKinney, W. (1998). In *Techniques of Vacuum Ultraviolet Physics*, edited by J. A. R. Samson and D. Ederer. Orlando: Academic Press.
Pianetta, P. (2009). Private communication.
Thieme, J. (1988). *X-ray Microscopy II, Springer Series in Optical Sciences*, edited by D. Sayre, M. R. Howells, J. Kirz and H. Rarback, pp. 70–79. Berlin: Springer-Verlag.
Xradia (2010). *DARPA Seedling Report* (subcontract GTS-S-10-1-008). Xradia, Pleasanton, CA, USA.
Zeng, X., Duewer, F., Feser, M., Huang, C., Lyon, A., Tkachuk, A. & Yun, W. (2008). *Appl. Opt.* **47**, 2376–2381.